

Finite boundary perturbation theory for the elastic equation of motion

Nozomu Takeuchi^{1,2}

¹*Earthquake Research Institute, University of Tokyo, Yayoi 1-1-1, Bunkyo-ku, Tokyo 113-0032, Japan. E-mail: takeuchi@eri.u-tokyo.ac.jp*

²*Seismological Laboratory, 215 McCone Hall, University of California, Berkeley, CA 94720-4760, USA*

Accepted 2004 December 23. Received 2004 December 20; in original form 2004 June 18

SUMMARY

In the waveform inversion for global 3-D heterogeneous mantle structure, it is critical to accurately compute the perturbation of synthetic seismograms caused by the crustal heterogeneities. In actual applications, to reduce the required CPU time, a weak form equation of motion in terms of global trial functions is widely used. For those trial functions, the principal difficulty is how to compute the effect of the perturbation in the location of boundaries (such as Moho and the surface). In previous studies, the formulation has been based on the first-order perturbation theory of the free oscillation. However, this method holds only for weakly heterogeneous media and for lower frequencies. In this study, we derive the exact weak form elastic equation of motion for finite boundary perturbations. Our method can be applied to arbitrary strongly heterogeneous media and to arbitrary frequencies, and should facilitate accurate crustal correction.

Key words: direct solution method, interior of the Earth, synthetic seismograms.

1 INTRODUCTION

The crust is the most heterogeneous region of the Earth and accurate crustal correction (i.e. accurate computation of the perturbation of synthetic seismograms caused by the crustal heterogeneities) is critical for obtaining accurate mantle structure models. The heterogeneities are usually represented by the summation of (i) the perturbation of physical properties (such as density and elastic constants) in the internal regions and (ii) the perturbation of the location of the boundaries (such as Moho and the surface), and the principal difficulty is how to compute the effect of the latter perturbation (e.g. Dahlen & Tromp 1998).

One popular solution is to use local trial functions. For example, the finite element method in terms of local trial functions (e.g. Lysmer & Drake 1972) and the spectrum element method (e.g. Priolo *et al.* 1994; Komatitsch & Vilotte 1998) can compute such an effect in a straightforward manner. Mizutani (2001) proposed an optimally accurate finite difference scheme (Geller & Takeuchi 1998; Takeuchi & Geller 2000) for the medium with arbitrary boundary shapes. Although forward computations up to higher frequencies for 3-D heterogeneous global Earth structure models have recently become feasible (e.g. Komatitsch & Tromp 2002a,b; Tsuboi *et al.* 2003), the required CPU time is intensive and the applications of such methods to global waveform inversion studies are still in the stage of becoming feasible.

The computational method applied to the actual waveform inversion studies for global 3-D Earth structure thus far has been either the modal summation method (e.g. Woodhouse & Dziewonski 1984; Li & Tanimoto 1993) or the direct solution method (e.g. Hara *et al.* 1993; Cummins *et al.* 1994; Geller & Ohminato 1994; Geller & Takeuchi 1995; Takeuchi *et al.* 1996; Cummins *et al.* 1997). Both methods solve the weak form equation of motion (or its equivalence) and use vector spherical harmonics as the laterally dependent part of the trial functions. If the structure model has only large-scale lateral heterogeneities, most of the matrix elements become zero because of the selection rule and, thus, the required CPU time to solve the equation of motion is greatly reduced.

Even for those global trial functions, accurate computation of the perturbed synthetic seismograms caused by the perturbation of physical properties (such as density and elastic constants) is straightforward. Direct solution of the equation of motion for laterally heterogeneous media (without using any perturbation approximations) is becoming feasible (e.g. Cummins *et al.* 1997). Higher order perturbation solutions (e.g. Lognonné & Romanowicz 1990; Takeuchi *et al.* 2000) have been proposed and the latter method ensures convergence. These solutions should allow highly accurate synthetic seismograms even for strongly heterogeneous media and for higher frequencies.

On the other hand, as for the perturbation of synthetic seismograms caused by the perturbation in the location of the boundaries, severe limitations still exist because previous solutions rely on the first-order perturbation theory of the free oscillation; Woodhouse (1976) and Woodhouse & Dahlen (1978) formulated a method to compute the perturbation of the eigenfrequencies, and Woodhouse (1980) extends these results to compute the perturbation of synthetic seismograms. They consider the infinitesimal perturbation of free oscillations in the vicinity of

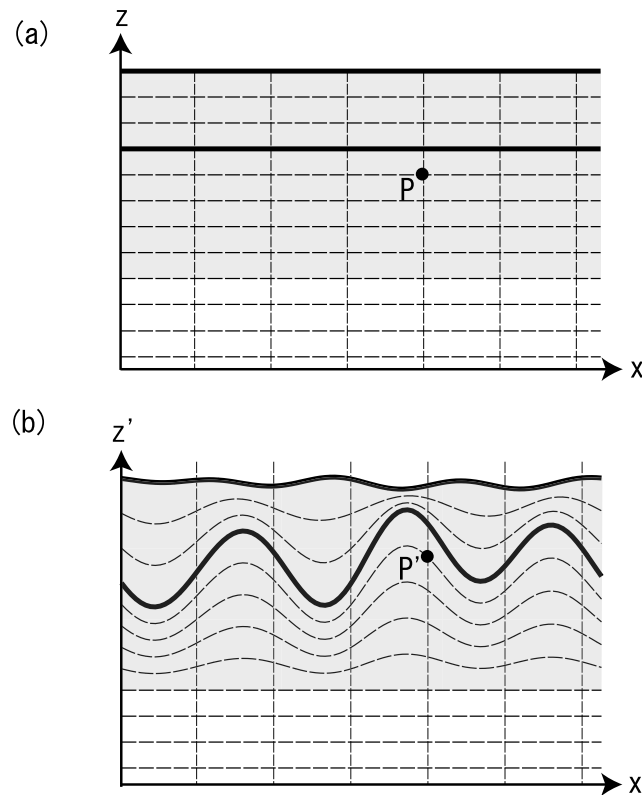


Figure 1. Schematic picture showing the one-to-one mapping between the initial model (a) and the perturbed model (b). Broken lines show the meshes of the mapping; the intersections of the mesh in the initial model are mapped to the corresponding intersection in the perturbed model (e.g. the position P is mapped to P'). Solid thick lines show the external and internal boundaries, and the shaded region shows the region deformed by the mapping.

the reference frequency: representative eigenfrequency of the considered modes. Thus, this method breaks down for strongly heterogeneous media or for higher frequencies.

In this study, we derive the exact weak form equation of motion for the medium with finite boundary perturbations. This method can be applied to arbitrary trial functions; that is, to both global and local trial functions. We can solve the derived equation of motion by either direct solution or higher order perturbation approximations, which allows highly accurate synthetic seismograms. We also show that we can derive the previous results by Woodhouse (1980) as a special case of our formulation.

2 THEORY

Following the conventions of previous studies, we formulate our theory in Cartesian coordinates. In this paper, we ignore the effect of self-gravity and Earth rotation.

2.1 Equation of motion and definition of the perturbation

First we write the equation of motion for both the initial model and the perturbed model. Following the convention of Woodhouse (1976), perturbation is expressed by one-to-one mapping between two models. The schematic relation is shown in Fig. 1. Figs 1(a) and (b) show the initial model and the perturbed model, respectively, and the intersections of meshes in Fig. 1(a) is mapped to the corresponding intersections in Fig. 1(b) (e.g. position P in the initial model is mapped to P' in the perturbed model).

As is obvious, the equation of motion is dependent on the choice of trial functions. In the perturbation theory of physical properties (such as the density and the elastic constants), we usually use the same trial functions for both the initial model and the perturbed model. However, in previous boundary perturbation theories (Woodhouse 1976; Woodhouse & Dahlen 1978; Woodhouse 1980), different trial functions are defined. Those trial functions are related by the mapping (as is shown later in eq. 8). Here, we follow this definition.

The weak form equation of motion for the initial model is as follows:

$$\omega^2 \int_V [\phi_i^{(m)}(\mathbf{x})]^* \rho(\mathbf{x}) u_i d\mathbf{x} - \int_V [\phi_{i,j}^{(m)}(\mathbf{x})]^* C_{ijkl}(\mathbf{x}) u_{k,l} d\mathbf{x} = - \int_V [\phi_i^{(m)}(\mathbf{x})]^* f_i(\mathbf{x}) d\mathbf{x}, \quad (1)$$

where ω is the frequency; u_i is the unknown wavefield for the initial model; $\phi_i^{(m)}$ is the trial function for the initial model; ρ , C_{ijkl} and f_i are the density, the elastic constant and the external force for the initial model, respectively; and V denotes the whole space of the initial model.

Here, we assume the Galerkin weak form: the weight functions are the complex conjugate of the trial functions (see, e.g. Geller & Ohminato 1994).

The weak form equation of motion for the perturbed model is as follows:

$$\omega^2 \int_{V'} [\phi_i^{(m)'}(\mathbf{x}')]^* \rho'(\mathbf{x}') u_i' d\mathbf{x}' - \int_{V'} [\phi_{i,j}^{(m)'}(\mathbf{x}')]^* C_{ijkl}'(\mathbf{x}') u_{k,l}' d\mathbf{x}' = - \int_{V'} [\phi_i^{(m)'}(\mathbf{x}')]^* f_i'(\mathbf{x}') d\mathbf{x}', \quad (2)$$

where u_i' is the unknown wavefield for the perturbed model; $\phi_i^{(m)'}$ is the trial function for the perturbed model; ρ' , C_{ijkl}' and f_i' are the density, the elastic constant and the external force for the perturbed model, respectively; and V' denotes the whole space of the perturbed model. Note that the trial functions used are different in eqs (1) and (2). We can use \mathbf{x} instead of \mathbf{x}' in eq. (2), but we use \mathbf{x}' for convenience in the later discussions.

Here, we denote the mapping between the two models as

$$\mathbf{x} \rightarrow \mathbf{x}'(\mathbf{x})$$

and we define the perturbed model as

$$\rho'(\mathbf{x}') = \rho(\mathbf{x}), \quad (3)$$

$$C_{ijkl}'(\mathbf{x}') = C_{ijkl}(\mathbf{x}), \quad (4)$$

$$f_i'(\mathbf{x}') d\mathbf{x}' = f_i(\mathbf{x}) d\mathbf{x}. \quad (5)$$

Note that all tensors (such as C_{ijkl}') and vectors (such as f_i') are expressed not in terms of oblique coordinates schematically as shown in Fig. 1(b), but in terms of Cartesian coordinates even for the perturbed model. The definitions of eqs (3) and (4) are different from those in previous theories. In these theories, they defined the mapping so that the boundaries in the initial model are mapped to the boundaries in the perturbed model (as in this paper) and assume that the physical properties between the two models are the same; i.e. the distribution of the density and the elastic constants are the same in the undeformed inner regions, and are smoothly extrapolated for the boundary regions. The resultant perturbed physical properties are given as

$$\rho''(\mathbf{x}') = \rho(\mathbf{x}) + \frac{\partial \rho}{\partial \mathbf{x}}(\mathbf{x})[\mathbf{x}'(\mathbf{x}) - \mathbf{x}], \quad (6)$$

$$C_{ijkl}''(\mathbf{x}') = C_{ijkl}(\mathbf{x}) + \frac{\partial C_{ijkl}}{\partial \mathbf{x}}(\mathbf{x})[\mathbf{x}'(\mathbf{x}) - \mathbf{x}], \quad (7)$$

to the first order. However, we adopt the definition of eqs (3) and (4) rather than eqs (6) and (7), because the smooth extrapolations in the latter leave ambiguity in the higher order terms for finite perturbations. Note that if we superimpose the appropriate perturbation of physical properties, we can express the perturbed model defined in the previous theories to the first order (see Section 3).

For the perturbed model of eqs (3)–(5), we define the trial function $\phi_i^{(m)'}$ by

$$\phi_i^{(m)'(\mathbf{x}')} = \phi_i^{(m)}(\mathbf{x}). \quad (8)$$

We discretize the unknown variable u_i in eq. (1) as

$$u_i(\mathbf{x}) = \sum_n c_n \phi_i^{(n)}(\mathbf{x}) \quad (9)$$

and u_i' in eq. (2) as

$$u_i'(\mathbf{x}') = \sum_n c_n' \phi_i^{(n)'(\mathbf{x}')}, \quad (10)$$

where c_n and c_n' are unknown expansion coefficients. Substituting eqs (9) and (10) into eqs (1) and (2), respectively, we obtain the following equation of motion in the matrix form:

$$(\omega^2 \mathbf{T} - \mathbf{H})\mathbf{c} = -\mathbf{g}, \quad (11)$$

$$(\omega^2 \mathbf{T}' - \mathbf{H}')\mathbf{c}' = -\mathbf{g}, \quad (12)$$

where

$$T_{mn} = \int_V [\phi_i^{(m)}(\mathbf{x})]^* \rho(\mathbf{x}) \phi_i^{(n)}(\mathbf{x}) d\mathbf{x}, \quad (13)$$

$$H_{mn} = \int_V [\phi_{i,j}^{(m)}(\mathbf{x})]^* C_{ijkl}(\mathbf{x}) \phi_{k,l}^{(n)}(\mathbf{x}) d\mathbf{x}, \quad (14)$$

$$T_{mn}' = \int_{V'} [\phi_i^{(m)'}(\mathbf{x}')]^* \rho'(\mathbf{x}') \phi_i^{(n)'(\mathbf{x}')} d\mathbf{x}', \quad (15)$$

$$H_{mn}' = \int_{V'} [\phi_{i,j}^{(m)'}(\mathbf{x}')]^* C_{ijkl}'(\mathbf{x}') \phi_{k,l}^{(n)'(\mathbf{x}')} d\mathbf{x}', \quad (16)$$

$$\mathbf{g}_m = \int_V [\phi_i^{(m)}(\mathbf{x})]^* f_i(\mathbf{x}) d\mathbf{x} = \int_{V'} [\phi_i^{(m)'}(\mathbf{x}')]^* f_i'(\mathbf{x}') d\mathbf{x}'. \quad (17)$$

Note that the right-hand side of eqs (11) and (12) are common because of eqs (5) and (8). Note also that the perturbation of synthetic seismograms, δu_i , obtained from $\delta \mathbf{c} (= \mathbf{c}' - \mathbf{c})$ is

$$\begin{aligned}
 \delta u_i(\mathbf{x}) &= \sum_n (c'_n - c_n) \phi_i^{(n)}(\mathbf{x}) \\
 &= \sum_n c'_n \phi_i^{(n)}(\mathbf{x}) - \sum_n c_n \phi_i^{(n)}(\mathbf{x}) \\
 &= \sum_n c'_n \phi_i^{(n)'}(\mathbf{x}') - \sum_n c_n \phi_i^{(n)}(\mathbf{x}) \\
 &= u'_i(\mathbf{x}') - u_i(\mathbf{x}) \\
 &\neq u'_i(\mathbf{x}) - u_i(\mathbf{x}).
 \end{aligned} \tag{18}$$

We use eq. (8) at the third line of eq. (18).

2.2 Explicit matrix elements

Next, we derive the explicit matrix elements of eqs (15) and (16) by using $\phi_i^{(n)}$, ρ and C_{ijkl} instead of $\phi_i^{(n)'}$, ρ' and C_{ijkl}' . In contrast to the previous studies, we do not use the first-order Born approximation. We denote the explicit elements of \mathbf{x} and \mathbf{x}' as $\mathbf{x} = (z, x, y)$ and $\mathbf{x}' = (z', x', y')$. Here, we assume the mapping between \mathbf{x} and \mathbf{x}' is expressed by

$$\begin{cases} z' = z + \delta Z(x, y, z) \\ x' = x \\ y' = y; \end{cases} \tag{19}$$

i.e. we assume the mapping is expressed by elevation as high as δZ . This expression cannot express all kinds of one-to-one mapping. Note, however, that we can express almost every boundary perturbation that appears in actual global seismological problems and, if we can once represent the boundary topography, we can represent arbitrary heterogeneous structure by superimposing the heterogeneities of physical properties. We will derive the matrix elements for general one-to-one mapping expressed by $\mathbf{x}' = \mathbf{x} + \delta \mathbf{X}(\mathbf{x})$ in the next subsection.

For \mathbf{x}' and \mathbf{x} of eq. (19), we can expect

$$\begin{bmatrix} dz' \\ dx' \\ dy' \end{bmatrix} = \begin{bmatrix} 1 + \delta Z_{,z} & \delta Z_{,x} & \delta Z_{,y} \\ 0 & 1 & 0 \\ 0 & 0 & 1 \end{bmatrix} \begin{bmatrix} dz \\ dx \\ dy \end{bmatrix}. \tag{20}$$

We integrate eq. (15) by substitution using eqs (3), (8) and (20), and we obtain

$$\begin{aligned}
 T'_{mn} &= \int_V [\phi_i^{(m)}(\mathbf{x})]^* \rho(\mathbf{x}) \phi_i^{(n)}(\mathbf{x}) \begin{vmatrix} 1 + \delta Z_{,z} & \delta Z_{,x} & \delta Z_{,y} \\ 0 & 1 & 0 \\ 0 & 0 & 1 \end{vmatrix} d\mathbf{x} \\
 &= \int_V [\phi_i^{(m)}(\mathbf{x})]^* \rho(\mathbf{x}) \phi_i^{(n)}(\mathbf{x}) (1 + \delta Z_{,z}) d\mathbf{x}.
 \end{aligned} \tag{21}$$

This is the mass matrix for the perturbed model. From eqs (13) and (21), we get

$$\delta T_{mn} = \int_V [\phi_i^{(m)}(\mathbf{x})]^* \rho(\mathbf{x}) \phi_i^{(n)}(\mathbf{x}) \delta Z_{,z} d\mathbf{x}, \tag{22}$$

where

$$\delta T_{mn} = T'_{mn} - T_{mn}. \tag{23}$$

To integrate eq. (16) by substitution, we need to relate $\phi_{i,j}^{(n)'}(\mathbf{x}')$ to $\phi_{i,j}^{(n)}(\mathbf{x})$. To do this, we should evaluate from which point $\lim_{\epsilon \rightarrow 0} (\mathbf{x}' + \epsilon \mathbf{e}_j)$ is mapped, where \mathbf{e}_j denotes the j th unit vector. From eq. (20), as $\epsilon \rightarrow 0$, we have

$$\mathbf{x} + \epsilon \mathbf{e}_{j'} \rightarrow \mathbf{x}' + \epsilon J_{jj'} \mathbf{e}_j, \tag{24}$$

where

$$[J_{jj'}] = \begin{bmatrix} 1 + \delta Z_{,z} & \delta Z_{,x} & \delta Z_{,y} \\ 0 & 1 & 0 \\ 0 & 0 & 1 \end{bmatrix}. \tag{25}$$

Thus, we have

$$\mathbf{x}' + \epsilon \mathbf{e}_j \leftarrow \mathbf{x} + \epsilon Q_{j'j} \mathbf{e}_{j'}, \tag{26}$$

where

$$[Q_{j'j}] = \begin{bmatrix} 1 + \delta Z_{,z} & \delta Z_{,x} & \delta Z_{,y} \\ 0 & 1 & 0 \\ 0 & 0 & 1 \end{bmatrix}^{-1} = \begin{bmatrix} 1 - \frac{\delta Z_{,z}}{1 + \delta Z_{,z}} & -\frac{\delta Z_{,x}}{1 + \delta Z_{,z}} & -\frac{\delta Z_{,y}}{1 + \delta Z_{,z}} \\ 0 & 1 & 0 \\ 0 & 0 & 1 \end{bmatrix}, \quad (27)$$

or

$$Q_{j'j} = \delta_{j'j} - \frac{\delta Z_{,j}}{1 + \delta Z_{,z}} \delta_{j'z}. \quad (28)$$

From eqs (26) and (28), we get

$$\mathbf{x}' + \epsilon \mathbf{e}_j \leftarrow \mathbf{x} + \epsilon \left(\delta_{j'j} - \frac{\delta Z_{,j}}{1 + \delta Z_{,z}} \delta_{j'z} \right) \mathbf{e}_{j'} \quad (29)$$

Using eqs (8) and (29), we get

$$\begin{aligned} \phi_{i,j}^{(m)'}(\mathbf{x}') &= \lim_{\epsilon \rightarrow 0} \frac{\phi_i^{(m)'}(\mathbf{x}' + \epsilon \mathbf{e}_j) - \phi_i^{(m)'}(\mathbf{x}')}{\epsilon} \\ &= \lim_{\epsilon \rightarrow 0} \frac{\phi_i^{(m)}[\mathbf{x} + \epsilon(\delta_{j'j} - \frac{\delta Z_{,j}}{1 + \delta Z_{,z}} \delta_{j'z}) \mathbf{e}_{j'}] - \phi_i^{(m)}(\mathbf{x})}{\epsilon} \\ &= \lim_{\epsilon \rightarrow 0} \frac{\phi_i^{(m)}(\mathbf{x} + \epsilon \mathbf{e}_j - \epsilon \frac{\delta Z_{,j}}{1 + \delta Z_{,z}} \mathbf{e}_z) - \phi_i^{(m)}(\mathbf{x})}{\epsilon} \\ &= \lim_{\epsilon \rightarrow 0} \frac{\phi_i^{(m)}(\mathbf{x}) + \epsilon \phi_{i,j}^{(m)}(\mathbf{x}) - \epsilon \frac{\delta Z_{,j}}{1 + \delta Z_{,z}} \phi_{i,z}^{(m)}(\mathbf{x}) - \phi_i^{(m)}(\mathbf{x})}{\epsilon} \\ &= \phi_{i,j}^{(m)}(\mathbf{x}) - \frac{\delta Z_{,j}}{1 + \delta Z_{,z}} \phi_{i,z}^{(m)}(\mathbf{x}). \end{aligned} \quad (30)$$

Integrating eq. (16) by substitution using eqs (4), (20) and (30), we get

$$H'_{mn} = \int_V \left[\phi_{i,j}^{(m)}(\mathbf{x}) - \frac{\delta Z_{,j}}{1 + \delta Z_{,z}} \phi_{i,z}^{(m)}(\mathbf{x}) \right]^* C_{ijkl}(\mathbf{x}) \left[\phi_{k,l}^{(n)}(\mathbf{x}) - \frac{\delta Z_{,l}}{1 + \delta Z_{,z}} \phi_{k,z}^{(n)}(\mathbf{x}) \right] (1 + \delta Z_{,z}) d\mathbf{x}. \quad (31)$$

This is the stiffness matrix for the perturbed model. From eqs (14) and (31), we obtain

$$\begin{aligned} \delta H_{mn} &= \int_V [\phi_{i,j}^{(m)}(\mathbf{x})]^* C_{ijkl}(\mathbf{x}) \phi_{k,l}^{(n)}(\mathbf{x}) \delta Z_{,z} d\mathbf{x} \\ &\quad - \int_V \{ [\phi_{i,z}^{(m)}(\mathbf{x})]^* C_{ijkl}(\mathbf{x}) \phi_{k,l}^{(n)}(\mathbf{x}) \delta Z_{,j} + [\phi_{i,j}^{(m)}(\mathbf{x})]^* C_{ijkl}(\mathbf{x}) \phi_{k,z}^{(n)}(\mathbf{x}) \delta Z_{,l} \} d\mathbf{x}, \\ &\quad + \int_V [\phi_{i,z}^{(m)}(\mathbf{x})]^* C_{ijkl}(\mathbf{x}) \phi_{k,z}^{(n)}(\mathbf{x}) \frac{\delta Z_{,j} \delta Z_{,l}}{1 + \delta Z_{,z}} d\mathbf{x}, \end{aligned} \quad (32)$$

where

$$\delta H_{mn} = H'_{mn} - H_{mn}. \quad (33)$$

Eqs (21) and (31) are the rigorous matrix elements and eqs (22) and (32) are the perturbation of matrix elements as a result of finite boundary perturbations. Note that we use neither the explicit value of $\phi_i^{(n)}$ nor the infinitesimal perturbation approximation, and thus these matrix elements hold for arbitrary trial functions and for arbitrary strongly heterogeneous media and arbitrary higher frequencies.

2.3 Explicit matrix elements: general case

Using procedures similar to those presented in the previous subsection, we can derive the matrix elements for the general one-to-one mapping given by

$$\mathbf{x}' = \mathbf{x} + \delta \mathbf{X}(\mathbf{x}). \quad (34)$$

The results are given by

$$T'_{mn} = \int_V [\phi_i^{(m)}(\mathbf{x})]^* \rho(\mathbf{x}) \phi_i^{(n)}(\mathbf{x}) |\mathbf{J}| d\mathbf{x}, \quad (35)$$

$$H'_{mn} = \int_V [Q_{j'j} \phi_{i,j}^{(m)}(\mathbf{x})]^* C_{ijkl}(\mathbf{x}) [Q_{l'l} \phi_{k,l}^{(n)}(\mathbf{x})] |\mathbf{J}| d\mathbf{x}, \quad (36)$$

where

$$J_{ij} = \delta_{ij} + \delta X_{i,j}, \quad (37)$$

$$Q_{ij} = (J_{ij})^{-1}. \quad (38)$$

Explicit elements of $|\mathbf{J}|$ and \mathbf{Q} in eqs (35) and (36) are directly computed from explicit evaluations of eqs (37) and (38), although the mathematics are tedious. Note that \mathbf{J} and \mathbf{Q} are known because δX_i are known variables.

3 FIRST-ORDER PERTURBATION THEORY

In this section, we derive the explicit matrix elements under the first-order Born approximation treating the perturbations, $\delta \mathbf{X}$ in eq. (34), as infinitesimal. Note that every equation in this section is to the first order. The independent variable for each function is \mathbf{x} unless explicitly stated otherwise. We assume that $\delta \mathbf{X}$ is derivable and its non-zero region is finite, and $\delta X_{i,j}$ are thus all first-order terms.

3.1 Explicit elements

As stated in Section 2.1, the distribution of the density and the elastic constants for the perturbed model differ between our theory and previous first-order perturbation theories. We derive the matrix elements for the perturbed model of the previous theories. We first evaluate the perturbation of our matrix elements, and then add the required perturbation resulting from different distributions of the density and elastic constants, i.e. the total perturbation of the matrix elements, δA_{mn} , is given as follows:

$$\delta A_{mn} = \omega^2 \delta T_{mn} - \delta H_{mn} + \omega^2 \int_V [\phi_i^{(m)}]^* \delta \rho' \phi_i^{(n)} d\mathbf{x} - \int_V [\phi_{i,j}^{(m)}]^* \delta C_{ijkl} \phi_{k,l}^{(n)} d\mathbf{x}, \quad (39)$$

where

$$\delta \rho'(\mathbf{x}) = \rho''[\mathbf{x}'(\mathbf{x})] - \rho'[\mathbf{x}'(\mathbf{x})], \quad (40)$$

$$\delta C_{ijkl}'(\mathbf{x}) = C_{ijkl}''[\mathbf{x}'(\mathbf{x})] - C_{ijkl}'[\mathbf{x}'(\mathbf{x})]. \quad (41)$$

First, we evaluate δT_{mn} and δH_{mn} in eq. (39) to the first order. From explicit evaluations of eqs (37) and (38), we get

$$|\mathbf{J}| = 1 + \delta X_{i,i}, \quad (42)$$

$$Q_{ij} = \delta_{ij} - \delta X_{i,j}. \quad (43)$$

Substituting eqs (42) and (43) into eqs (35) and (36), we get

$$T'_{mn} = \int_V [\phi_i^{(m)}]^* \rho \phi_i^{(n)} (1 + \delta X_{p,p}) d\mathbf{x}, \quad (44)$$

$$H'_{mn} = \int_V [\phi_{i,j}^{(m)} - \delta X_{j',j} \phi_{i,j'}^{(m)}]^* C_{ijkl} [\phi_{k,l}^{(n)} - \delta X_{l',l} \phi_{k,l'}^{(n)}] (1 + \delta X_{p,p}) d\mathbf{x}. \quad (45)$$

Substituting eqs (13), (14), (44) and (45) into eqs (23) and (33), we get

$$\delta T_{mn} = \int_V [\phi_i^{(m)}]^* \rho \phi_i^{(n)} \delta X_{p,p} d\mathbf{x}, \quad (46)$$

$$\begin{aligned} \delta H_{mn} = & \int_V [\phi_{i,j}^{(m)}]^* C_{ijkl} \phi_{k,l}^{(n)} \delta X_{p,p} d\mathbf{x} \\ & - \int_V \{ [\phi_{i,j'}^{(m)}]^* C_{ijkl} \phi_{k,l}^{(n)} + \phi_{i,j'}^{(n)} C_{ijkl} [\phi_{k,l}^{(m)}]^* \} \delta X_{j',j} d\mathbf{x}. \end{aligned} \quad (47)$$

In deriving the last term of eq. (47), we use the symmetric nature of C_{ijkl} : i.e. $C_{ijkl} = C_{klij}$.

Next, we add the required perturbation of the density and the elastic constants. Substituting eqs (3), (4), (6) and (7) into eqs (40) and (41), we can see the required perturbations are

$$\delta \rho'(\mathbf{x}) = \frac{\partial \rho}{\partial \mathbf{x}}(\mathbf{x})[\mathbf{x}'(\mathbf{x}) - \mathbf{x}], \quad (48)$$

$$\delta C_{ijkl}'(\mathbf{x}) = \frac{\partial C_{ijkl}}{\partial \mathbf{x}}(\mathbf{x})[\mathbf{x}'(\mathbf{x}) - \mathbf{x}]. \quad (49)$$

Substituting eq. (34) into eqs (48) and (49), we get

$$\delta \rho' = \rho_{,p} \delta X_p, \quad (50)$$

$$\delta C_{ijkl}' = C_{ijkl,p} \delta X_p. \quad (51)$$

Substituting eqs (46), (47), (50) and (51) into eq. (39), we get

$$\begin{aligned}
\delta A_{mn} = & \omega^2 \int_V [\phi_i^{(m)}]^* \rho \phi_i^{(n)} \delta X_{p,p} d\mathbf{x} \\
& - \int_V [\phi_{i,j}^{(m)}]^* C_{ijkl} \phi_{k,l}^{(n)} \delta X_{p,p} d\mathbf{x} \\
& + \int_V \{ [\phi_{i,p}^{(m)}]^* C_{ijkl} \phi_{k,l}^{(n)} + \phi_{i,p}^{(n)} C_{ijkl} [\phi_{k,l}^{(m)}]^* \} \delta X_{p,j} d\mathbf{x} \\
& + \omega^2 \int_V [\phi_i^{(m)}]^* \rho_p \phi_i^{(n)} \delta X_p d\mathbf{x} - \int_V [\phi_{i,j}^{(m)}]^* C_{ijkl,p} \phi_{k,l}^{(n)} \delta X_p d\mathbf{x}.
\end{aligned} \tag{52}$$

Note that we exchange the indices ($j' \rightarrow p$ and $l' \rightarrow p$) and use the symmetric nature of C_{ijkl} in the third line of eq. (52). Integrating the first three terms of right-hand side of eq. (52) by parts, we obtain

$$\begin{aligned}
\delta A_{mn} = & \int_S \{ \omega^2 [\phi_i^{(m)}]^* \rho \phi_i^{(n)} - [\phi_{i,j}^{(m)}]^* C_{ijkl} \phi_{k,l}^{(n)} \} \delta X_p n_p dS \\
& + \int_S \{ [\phi_{i,p}^{(m)}]^* C_{ijkl} \phi_{k,l}^{(n)} + \phi_{i,p}^{(n)} C_{ijkl} [\phi_{k,l}^{(m)}]^* \} \delta X_p n_j dS \\
& - \int_V \{ \omega^2 [\phi_i^{(m)}]^* \rho \phi_i^{(n)} - [\phi_{i,j}^{(m)}]^* C_{ijkl} \phi_{k,l}^{(n)} \}_{,p} \delta X_p d\mathbf{x} \\
& - \int_V \{ [\phi_{i,p}^{(m)}]^* C_{ijkl} \phi_{k,l}^{(n)} + \phi_{i,p}^{(n)} C_{ijkl} [\phi_{k,l}^{(m)}]^* \}_{,j} \delta X_p d\mathbf{x} \\
& + \omega^2 \int_V [\phi_i^{(m)}]^* \rho_p \phi_i^{(n)} \delta X_p d\mathbf{x} - \int_V [\phi_{i,j}^{(m)}]^* C_{ijkl,p} \phi_{k,l}^{(n)} \delta X_p d\mathbf{x} \\
= & \int_S \{ \omega^2 [\phi_i^{(m)}]^* \rho \phi_i^{(n)} - [\phi_{i,j}^{(m)}]^* C_{ijkl} \phi_{k,l}^{(n)} \} \delta X_p n_p dS \\
& + \int_S \{ [\phi_{i,p}^{(m)}]^* C_{ijkl} \phi_{k,l}^{(n)} + \phi_{i,p}^{(n)} C_{ijkl} [\phi_{k,l}^{(m)}]^* \} \delta X_p n_j dS \\
& - \int_V [\phi_{i,p}^{(m)}]^* \{ \rho \omega^2 \phi_i^{(n)} + [C_{ijkl} \phi_{k,l}^{(n)}]_{,j} \} \delta X_p d\mathbf{x} \\
& - \int_V \phi_{i,p}^{(n)} \{ \rho \omega^2 [\phi_i^{(m)}]^* + [C_{ijkl} [\phi_{k,l}^{(m)}]^*]_{,j} \} \delta X_p d\mathbf{x},
\end{aligned} \tag{53}$$

where S represents the internal and external surfaces in V and n_j is the unit normal vector of the surface.

3.2 Multiplet coupling problem

Now we consider the matrix elements of eq. (53) for the multiplet coupling problem in the vicinity of the reference frequency and show the obtained elements, which are the same as those in Woodhouse (1980). We assume we use the eigenfunctions $s_i^{(n)}$ as trial functions $\phi_i^{(n)}$. In this subsection only, we assume an elastic Earth model (i.e. C_{ijkl} are real). We denote the reference frequency as ω_0 . For this multiplet coupling problem, the matrix elements of eq. (53) are as follows:

$$\begin{aligned}
\delta A_{mn} = & \int_S \{ \omega_0^2 [s_i^{(m)}]^* \rho s_i^{(n)} - [s_{i,j}^{(m)}]^* C_{ijkl} s_{k,l}^{(n)} \} \delta X_p n_p dS \\
& + \int_S \{ [s_{i,p}^{(m)}]^* C_{ijkl} s_{k,l}^{(n)} + s_{i,p}^{(n)} C_{ijkl} [s_{k,l}^{(m)}]^* \} \delta X_p n_j dS.
\end{aligned} \tag{54}$$

Note that the last two terms of eq. (53) disappear because $s_i^{(n)}$ satisfies the homogeneous equation of motion and

$$\rho \omega^2 s_i^{(n)} + [C_{ijkl} s_{k,l}^{(n)}]_{,j} = 0(\epsilon^2), \tag{55}$$

$$\rho \omega^2 [s_i^{(m)}]^* + \{ C_{ijkl} [s_{k,l}^{(n)}]^* \}_{,j} = 0(\epsilon^2), \tag{56}$$

when $\omega - \omega_0 = O(\epsilon)$. If we denote the amplitude of boundary perturbation in the normal direction (from $-$ to $+$) as δh , then δX_p is given as

$$\delta X_p = \delta h n_p^+ \tag{57}$$

on the surface S , where n_p^+ is the normal vector of the surface from $-$ to $+$. Substituting eq. (57) into eq. (54), we obtain

$$\begin{aligned}
\delta A_{mn} &= \int_S \left\{ \omega_0^2 [s_i^{(m)}]^* \rho s_i^{(n)} - [s_{i,j}^{(m)}]^* C_{ijkl} s_{k,l}^{(n)} \right\} \delta h n_p^+ n_p dS \\
&\quad + \int_S \left\{ [s_{i,p}^{(m)}]^* C_{ijkl} s_{k,l}^{(n)} + s_{i,p}^{(n)} C_{ijkl} [s_{k,l}^{(m)}]^* \right\} \delta h n_p^+ n_j dS \\
&= - \int_S \left\{ \omega_0^2 [s_i^{(m)}]^* \rho s_i^{(n)} - [s_{i,j}^{(m)}]^* C_{ijkl} s_{k,l}^{(n)} \right\}^+ \delta h dS \\
&\quad - \int_S \left\{ [s_{i,p}^{(m)}]^* C_{ijkl} s_{k,l}^{(n)} + s_{i,p}^{(n)} C_{ijkl} [s_{k,l}^{(m)}]^* \right\}^+ \delta h n_p^+ n_j^+ dS.
\end{aligned} \tag{58}$$

These are the matrix elements given in Woodhouse (1980), which are derived from eq. (18) of Woodhouse (1976).

4 NUMERICAL SOLUTION

4.1 Matrix elements in terms of the fourier basis

We derive the perturbation of the matrix elements in eqs (22) and (32) resulting from finite boundary perturbations. Here, we discuss how to evaluate these matrix elements when we use global functions (such as the discrete Fourier basis and spherical harmonics) as the horizontally dependent part of the trial functions. In this subsection, we first show the explicit formulations for a 2-D *SH* problem in terms of the discrete Fourier basis. We show that if the matrix elements are rigorously evaluated, we obtain huge numbers of non-zero elements and require huge CPU time to solve the equation of motion in eq. (12). We incorporate some approximations to greatly reduce the non-zero elements and, thereby, the required CPU time.

We assume the problem (the structure, the source and the wavefield) is homogeneous in the y direction for both the initial model and the perturbed model. We denote the rigidity as μ . We use the laterally homogeneous initial model: the density ρ and the rigidity μ are a function of z only. We assume the whole space is a rectangle whose measurements are L_x and L_z in the x and z directions, respectively. For this problem, the matrix operators for the initial model (eqs 13 and 14) are as follows:

$$T_{mn} = \int_0^{L_z} \int_0^{L_x} [\phi^{(m)}]^* \rho \phi^{(n)} dx dz, \tag{59}$$

$$H_{mn} = \int_0^{L_z} \int_0^{L_x} [\phi_{,x}^{(m)}]^* \mu \phi_{,x}^{(n)} dx dz + \int_0^{L_z} \int_0^{L_x} [\phi_{,z}^{(m)}]^* \mu \phi_{,z}^{(n)} dx dz. \tag{60}$$

The perturbation of the matrix operators (eqs 22 and 32) as a result of the perturbation, δZ in eq. (19), is as follows:

$$\delta T_{mn} = \int_0^{L_z} \int_0^{L_x} [\phi^{(m)}]^* \rho \phi^{(n)} \delta Z_{,z} dx dz, \tag{61}$$

$$\begin{aligned}
\delta H_{mn} &= \int_0^{L_z} \int_0^{L_x} [\phi_{,x}^{(m)}]^* \mu \phi_{,x}^{(n)} \delta Z_{,z} dx dz - \int_0^{L_z} \int_0^{L_x} [\phi_{,z}^{(m)}]^* \mu \phi_{,z}^{(n)} \delta Z_{,z} dx dz \\
&\quad - \int_0^{L_z} \int_0^{L_x} [\phi_{,z}^{(m)}]^* \mu \phi_{,x}^{(n)} \delta Z_{,x} dx dz - \int_0^{L_z} \int_0^{L_x} [\phi_{,x}^{(m)}]^* \mu \phi_{,z}^{(n)} \delta Z_{,x} dx dz \\
&\quad + \int_0^{L_z} \int_0^{L_x} [\phi_{,z}^{(m)}]^* \mu \phi_{,z}^{(n)} \frac{\delta Z_{,x} \delta Z_{,x} + \delta Z_{,z} \delta Z_{,z}}{1 + \delta Z_{,z}} dx dz.
\end{aligned} \tag{62}$$

Here, we show how to evaluate eqs (61) and (62) when we use the trial functions

$$\phi^{(n)}(x, z) = W^{(q)}(z) \Phi^{(\alpha)}(x), \tag{63}$$

where (n) is the index to denote a pair of indices (q, α) , $W^{(q)}$ represents the vertically dependent part of the trial functions (e.g. the linear spline functions) and $\Phi^{(\alpha)}$ represents the discrete Fourier basis:

$$\Phi^{(\alpha)}(x) = \exp(i\alpha \Delta k_x x) \quad \left(\Delta k_x = \frac{2\pi}{L_x} \right). \tag{64}$$

In a manner similar to that of the popular approach for the perturbation of the physical properties, we parametrize the perturbation, δZ in eq. (19), in terms of appropriate basis functions. In our method, we expand in terms of the linear spline functions for the vertically dependent part and the discrete Fourier basis for the horizontally dependent part, as follows:

$$\delta Z(x, z) = \sum_{k=0}^K \sum_{s=-s_{\max}}^{s_{\max}} \delta z_{ks} X^{(k)}(z) \Phi^{(s)}(x), \tag{65}$$

where s_{\max} is the maximum order of the Fourier series to express the perturbation, δz_{ks} are the expansion coefficients, $X^{(k)}$ are linear spline

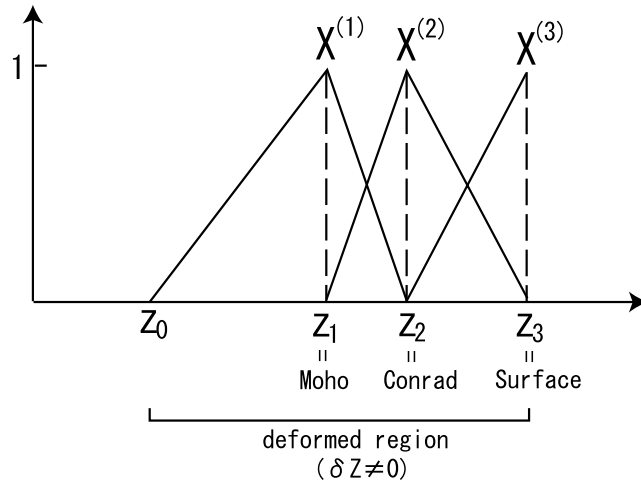


Figure 2. The linear spline function system $X^{(k)}(z)$ used in the expansion of eq. (65) when the deformed region (the region where δZ is non-zero) is only in a part of the space ($z \geq z_0$) and the deformed boundaries are the Moho (at $z = z_1$), the Conrad (at $z = z_2$) and the surface (at $z = z_3$).

functions

$$X^{(k)}(z) = \begin{cases} \frac{z - z_{k-1}}{z_k - z_{k-1}} & (z_{k-1} \leq z \leq z_k) \\ \frac{z_{k+1} - z}{z_{k+1} - z_k} & (z_k \leq z \leq z_{k+1}) \\ 0 & (\text{otherwise}) \end{cases} \quad (66)$$

and K is the maximum of k . We neglect the first and the second line of eq. (66) for the $k = 0$ and $k = K$ cases, respectively. Note that $W^{(q)}(z)$ in eq. (63) and $X^{(k)}(z)$ in eq. (65) are distinct sets. We have various choices for the vertically dependent part of the basis functions in eq. (65), but we use the linear spline functions because they give the simplest results in the formulations below. Here, we assume the deformed region (the region where δZ is non-zero) spreads throughout the whole space.

When the deformed region is only in a portion of the space, we define a different linear spline function system. For example, if we perturb only the Moho, the Conrad and the surface (or the bathymetry; note that liquid regions such as oceans are excluded from the *SH* problem), we use the linear spline functions shown in Fig. 2. We assume the deformed region is only $z \geq z_0$, and the locations of the Moho, the Conrad and the surface are $z = z_1$, $z = z_2$ and $z = z_3$, respectively. For this case, we do not use $X^{(0)}$ to ensure the continuity of δZ and define $X^{(1)} - X^{(3)}$ whose node is $z_1 - z_3$, respectively. It is useful to use the linear spline functions, not restricted to this case, whose node coincides with the location of the discontinuities because the expansion coefficients δz_{ks} in eq. (65) represent the spectrum of the elevation at the discontinuities: i.e. the spectrum of the topography of the discontinuities. In the formulations below, we show the matrix elements of eqs (61) and (62) for δZ in terms of eqs (65) and (66). Some modifications are required if we are to use the linear spline functions in Fig. 2, but the modifications are very minor.

The use of the trial functions of eq. (64) is efficient when we can use the selection rule in this problem:

$$\int_0^{L_x} [\Phi^{(\alpha')}]^* \Phi^{(s)} \Phi^{(\alpha)} dx = \begin{cases} L_x & (\text{if } -\alpha' + s + \alpha = 0) \\ 0 & (\text{otherwise}). \end{cases} \quad (67)$$

However, if we substitute eqs (63)–(65) into eqs (61) and (62), we see that a huge number of non-zero elements in $\delta \mathbf{H}$ arise because we have a term non-linear to δZ (i.e. the last term in right-hand side of eq. 62). To fully utilize the merit of the selection rule, we use the approximation to re-expand the non-linear term in terms of the discrete Fourier basis, as follows:

$$\frac{\delta Z_{,x} \delta Z_{,x} + \delta Z_{,z} \delta Z_{,z}}{1 + \delta Z_{,z}} = \sum_{k'} \sum_{s'=-s'_{\max}}^{s'_{\max}} \delta z'_{k's'} P^{(k')}(z) \Phi^{(s')}(x), \quad (68)$$

where $\delta z'_{k's'}$ are the expansion coefficients of this non-linear term and $P^{(k')}$ is some z -dependent function used in the expansion (we give the explicit form later in eqs 74–77). Using the trial functions of eq. (63) and the expansion of eqs (65) and (68), the matrix elements of eqs (61) and (62) are as follows:

$$\delta T_{mn} = \sum_{k,s} L_x \delta_{\alpha',s+\alpha} \delta z_{ks} \int_0^{L_z} W^{(q')} \rho W^{(q)} \frac{dX^{(k)}}{dz} dz, \quad (69)$$

$$\begin{aligned}
\delta H_{mn} = & \sum_{k,s} \alpha' \alpha \Delta k_x^2 L_x \delta_{\alpha',s+\alpha} \delta z_{ks} \int_0^{L_z} W^{(q')} \mu W^{(q)} \frac{dX^{(k)}}{dz} dz \\
& - \sum_{k,s} L_x \delta_{\alpha',s+\alpha} \delta z_{ks} \int_0^{L_z} \frac{dW^{(q')}}{dz} \mu \frac{dW^{(q)}}{dz} \frac{dX^{(k)}}{dz} dz \\
& + \sum_{k,s} s \alpha \Delta k_x^2 L_x \delta_{\alpha',s+\alpha} \delta z_{ks} \int_0^{L_z} \frac{dW^{(q')}}{dz} \mu W^{(q)} X^{(k)} dz \\
& - \sum_{k,s} \alpha' s \Delta k_x^2 L_x \delta_{\alpha',s+\alpha} \delta z_{ks} \int_0^{L_z} W^{(q')} \mu \frac{dW^{(q)}}{dz} X^{(k)} dz \\
& + \sum_{k',s'} L_x \delta_{\alpha',s'+\alpha} \delta z'_{k's'} \int_0^{L_z} \frac{dW^{(q')}}{dz} \mu \frac{dW^{(q)}}{dz} P^{(k')} dz,
\end{aligned} \tag{70}$$

where (m) is the index to denote a pair of indices (q', α') . We see that the selection rule of eq. (67) is fully utilized and most of the matrix elements are zero if s'_{\max} in eq. (68) is reasonably small. It is well known that for smooth media (i.e. if we can well approximate the perturbation by the expansion of eq. 65 by smaller s_{\max}), we can approximate the wavefield by considering only coupling between nearby wavenumbers and the truncation in eq. (68) should be a reasonable approximation. We show that this approximation works fine for actual applications in the numerical examples below. The accuracy of the obtained solution increases as s'_{\max} becomes larger, but the required CPU time also increases. In the actual application, we should choose an appropriate s'_{\max} considering the trade-off between accuracy and CPU time.

The remaining questions are how to choose $P^{(k')}(z)$ and how to determine $\delta z'_{k's'}$ in eq. (68). We can straightforwardly determine $P^{(k')}$ and $\delta z'_{k's'}$ by explicit evaluations. Substituting the explicit form of eqs (65) and (66), we get

$$\begin{aligned}
\frac{\delta Z_{,x} \delta Z_{,x} + \delta Z_{,z} \delta Z_{,z}}{1 + \delta Z_{,z}} = & X^{(k-1)2}(z) \frac{F^{(k-1)2}(x)}{1 + G^{(k)}(x)} + X^{(k)2}(z) \frac{F^{(k)2}(x)}{1 + G^{(k)}(x)} \\
& + 2X^{(k-1)}(z)X^{(k)}(z) \frac{F^{(k-1)}(x)F^{(k)}(x)}{1 + G^{(k)}(x)} + \frac{G^{(k)2}(x)}{1 + G^{(k)}(x)}
\end{aligned} \tag{71}$$

in $z_{k-1} \leq z \leq z_k$, where

$$F^{(k)}(x) = \sum_s \delta z_{ks} \Phi_x^{(s)}(x), \tag{72}$$

$$G^{(k)}(x) = \frac{-\sum_s \delta z_{(k-1)s} \Phi^{(s)}(x) + \sum_s \delta z_{ks} \Phi^{(s)}(x)}{z_k - z_{k-1}} \tag{73}$$

and $1 \leq k \leq K$. Comparing eqs (68) and (71), we see that $P^{(k')}$ and $\delta z'_{k's'}$ are as follows:

$$P^{(4k+1)}(z) = \begin{cases} X^{(k-1)2}(z) & (z_{k-1} \leq z \leq z_k) \\ 0 & (\text{otherwise}), \end{cases} \tag{74}$$

$$P^{(4k+2)}(z) = \begin{cases} X^{(k)2}(z) & (z_{k-1} \leq z \leq z_k) \\ 0 & (\text{otherwise}), \end{cases} \tag{75}$$

$$P^{(4k+3)}(z) = \begin{cases} 2X^{(k-1)}(z)X^{(k)}(z) & (z_{k-1} \leq z \leq z_k) \\ 0 & (\text{otherwise}), \end{cases} \tag{76}$$

$$P^{(4k+4)}(z) = \begin{cases} 1 & (z_{k-1} \leq z \leq z_k) \\ 0 & (\text{otherwise}), \end{cases} \tag{77}$$

$$\delta z'_{(4k+1)s'} = \frac{1}{L_x} \int [\Phi^{(s')}(x)]^* \frac{F^{(k-1)2}(x)}{1 + G^{(k)}(x)} dx, \tag{78}$$

$$\delta z'_{(4k+2)s'} = \frac{1}{L_x} \int [\Phi^{(s')}(x)]^* \frac{F^{(k)2}(x)}{1 + G^{(k)}(x)} dx, \tag{79}$$

$$\delta z'_{(4k+3)s'} = \frac{1}{L_x} \int [\Phi^{(s')}(x)]^* \frac{F^{(k-1)}(x)F^{(k)}(x)}{1 + G^{(k)}(x)} dx, \tag{80}$$

$$\delta z'_{(4k+4)s'} = \frac{1}{L_x} \int [\Phi^{(s')}(x)]^* \frac{G^{(k)2}(x)}{1 + G^{(k)}(x)} dx. \tag{81}$$

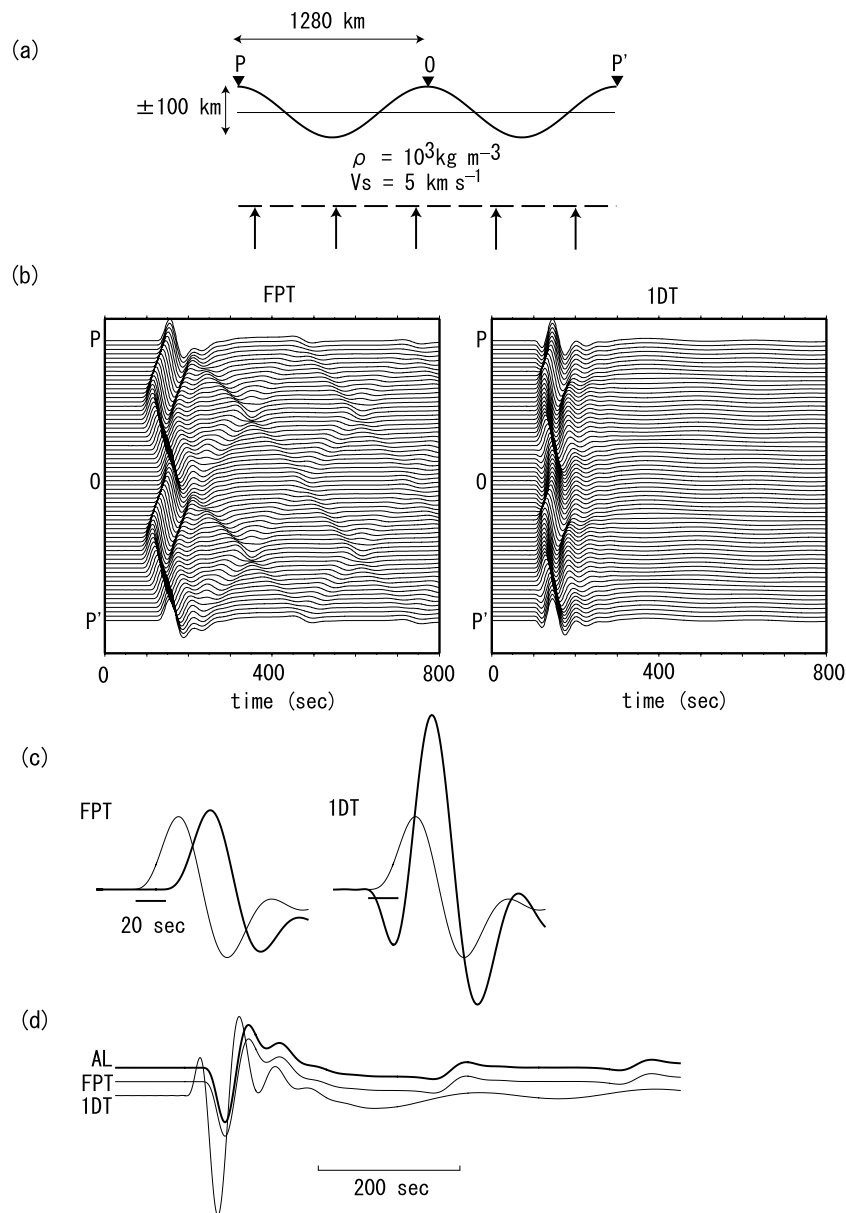


Figure 3. (a) The initial model (thin solid line) and the perturbed model (thick solid line) used in this simulation. The broken line shows the wavefront of the incident plane wave. P , O and P' are the locations of the receiver in the record section of (b). (b) The record section computed by using finite perturbation theory (FPT; left) and first-order perturbation theory (1DT; right) for the perturbed model shown in (a). The amplitude is normalized by the maximum amplitude of each trace. (c) The synthetic seismograms for the initial model (thin line) and for the perturbed model (thick solid line) for the receiver O computed by using FPT (left) and 1DT (right). (d) Comparison of the synthetic seismograms for the perturbed model for the receiver O computed using Aki & Larner's method (top; labelled as AL), FPT (middle) and 1DT (bottom).

4.2 Numerical examples

In this subsection, we show that our finite perturbation theory (hereafter referred as FPT) can compute the effect of crustal heterogeneities much more accurately than can the existing first-order perturbation theory (hereafter referred to as 1DT). We consider 2-D SH problems and use the trial functions of eq. (63). The FPT matrix elements for the perturbed models are eqs (61) and (62). In evaluating eq. (62), we do not use the approximation of eq. (68) but consider all couplings between every pair of trial functions used and the error in FPT is only the result of the use of a finite number of trial functions. We also compute a synthetic seismogram by using FPT with the approximation of eq. (68), compare it to the synthetic seismograms computed by FPT with consideration of all couplings and thereby show that our approximation is reasonable.

First, we show a simple example to demonstrate the accuracy of FPT and the inaccuracy of 1DT. Fig. 3(a) shows the medium we consider here. We consider a homogeneous initial model with the density $\rho = 10^3 \text{ kg m}^{-3}$ and the velocity $V_s = 5 \text{ km s}^{-1}$ (i.e. $\mu = 25 \text{ GPa}$). We consider the perturbed model with 100 km perturbation in the surface topography whose wavelength is 1280 km. We consider the vertical incident plane wave. Fig. 3(b) shows the computed synthetic seismograms for the perturbed model. The left synthetic seismograms are computed by

FPT, the right synthetic seismograms by 1DT. We applied a bandpass filter with corner frequencies of 1/1000 and 1/50 Hz. The receivers are aligned at each 40 km and the synthetic seismograms for the receivers P , O and P' in Fig. 3(a) are explicitly labelled in Fig. 3(b). Fig. 3(c) shows the enlarged waveforms of the first motion part for the receiver O . We can see two distinct discrepancies between the FPT and 1DT synthetic seismograms.

One discrepancy, as can be seen in Fig. 3(c), is that the amount of both phase and amplitude perturbations do not agree between these two methods. The 1DT synthetic seismogram has a smaller phase shift and a much larger amplitude perturbation. We see that the 1DT synthetic seismograms are inaccurate and the FPT synthetic seismograms are accurate for the following reasons. The phase perturbation can be predicted by using the ray theory. Because we have a 100-km bump at the receiver O , we expect a 20-s phase delay. Fig. 3(c) clearly shows that the FPT can compute the expected phase delay but 1DT cannot. It is well known that the phase shift computed by the first-order perturbation theory saturates at $\pi/4$. Actually, a 20-s delay is larger than the $\pi/4$ phase shift (12.5 s for the dominant frequency) and the 1DT synthetic seismogram has a phase shift of almost $\pi/4$. For the amplitude perturbation, we expect a focusing effect caused by the topography. However, because the wavelength of the topography (1280 km) is much larger than the wavelength of the wavefield (250 km for the dominant frequency), the effect should be small. Fig. 3(c) shows that FPT can model such amplitude perturbation but 1DT cannot.

The other discrepancy is that, as can be seen in Fig. 3(b), only FPT synthetic seismograms have clear later phases. These later phases are scattering waves as a result of the surface topographies. The surface topography should produce scattering waves and the lack of such scattering waves shows the limitation of 1DT.

If we compare these synthetic seismograms to synthetic seismograms computed by a different method, we can directly confirm the validity of FPT. We computed synthetic seismograms for the same problem using the method presented by Aki & Larner (1970; hereafter referred as AL). We assumed that the medium in Fig. 3(a) consists of two homogeneous layers with the same density and velocity. We also assumed that the interface between these layers is flat. Under these assumptions, it is rigorously true that the incident wave is the only upgoing wave in the second (deeper) layer and we could thus avoid the Rayleigh ansatz error, which appears in the original formulation of AL. To solve this two-layer problem, we made modifications to the original formulation equivalent to those by Kohketsu (1987). Fig. 3(d) shows a comparison of the synthetic seismograms for the perturbed model for the receiver O computed by AL, FPT and 1DT. We observed remarkable agreement between the synthetic seismogram computed by FPT and that computed by AL, while that computed by 1DT was completely different. If we assume that the AL synthetic seismogram is exact, the waveform error (see eq. 5.4 of Geller & Takeuchi 1995) of the FPT synthetic seismogram was only 0.417 per cent, while that of the 1DT synthetic seismogram was 134 per cent.

Next, we show that in the simulations of more realistic problems, a similar breakdown can be observed in 1DT synthetic seismograms. We consider a plane of a great circle including the path shown by the solid line in Fig. 4(a) and simulate SH waves propagating on this plane by solving the 2-D SH problem in Cartesian coordinates.

We apply the Earth flattening transformation to the modified isotropic PREM (Preliminary Reference Earth Model; Dziewonski & Anderson 1981) and use it as an initial model. We replace the S velocity model in Moho 220 km depth of the isotropic PREM with the SH velocity model (propagating perpendicular to the axis of symmetry) of the anisotropic PREM. We apply the Earth flattening transformation to the topography of the surface (or the bathymetry), the Conrad and the Moho of the Crust 2.0 model (Bassin *et al.* 2000) on the solid line in Fig. 4(a) (5120 km long), assume the topographies are symmetric with respect to the star in Fig. 4(a) and expand those 10 240-km-long topographies in terms of the Fourier basis up to degree 24. The resultant topographies are shown in Fig. 4(b) (note that we only show the right half of the considered medium) and the minimum wavelength of the topography in this model is 10 240/24 km, which is comparable to the resolution of the Crust 2.0 model. We define the perturbed model by δZ in eq. (65) whose expansion coefficients δz_{ks} are the spectrum of the above topography model. Thus, the s_{\max} in eq. (65) is 24. Here, we use the linear spline function system in Fig. 2 and set the boundary of the deformed region at a depth of 80 km (i.e. z_0 in Fig. 2 is set to the Earth flattening transformed position of 80 km depth).

We consider a line source on the Conrad at the place indicated by the star in Fig. 4(a). We assume the force system applied is a single force that is perpendicular to the plane of the great circle. This source is not realistic but, because our concern here is to mimic the amount of phase and amplitude perturbations and to mimic the effect of the couplings between different wavenumbers, the use of this source will not affect the conclusion in this subsection. We compute synthetic seismograms for the initial model and the perturbed model, and show the record sections in Fig. 4(c). For the perturbed model, we compute by using FPT and 1DT, respectively. We plot the synthetic seismograms at the surface at every 80 km between $0 \leq x \leq 2960$ km, where x represents the distance from the epicentre. We apply a bandpass filter with the corner frequencies of 1/1000 and 1/50 Hz. In the record section for the initial model (Fig. 4c left), as well as the body waves observed at the first motion part, we observe the Love waves traveling at a speed of approximately 4.4 km s^{-1} (aligning almost straight in the record section). Their waveforms are almost one wave packet and do not clearly show dispersion. On the other hand, in the record section computed for the perturbed model by using FPT (Fig. 4c middle), we observe Love waves with clear dispersion. For example, at $x = 2960$ km, Love waves last for approximately 400 s and dominant frequencies become higher as time goes on. This is a well-known feature of Love waves traveling through a continent. Because Love waves of higher frequencies are more greatly affected by crustal heterogeneity, they have a greater phase delay as a result of the crustal thickening. On the other hand, the surface waves of lower frequencies are less affected by the crustal heterogeneities. Thus, we have the Love waves with clear dispersion. However, in the record section computed for the perturbed model by using 1DT (Fig. 4c right), we cannot clearly see dispersion, an indication that 1DT breaks down for this frequency range.

The breakdown of 1DT is also confirmed if we compare the amount of the phase and the amplitude perturbation in each trace. Fig. 4(d) shows the comparison between the synthetic seismograms for the initial model and those for the perturbed model at $x = 2960$ km. Using FPT, we observe a phase shift over $\pi/4$, while the amplitude perturbation is not so large. However, using 1DT, we see a phase shift of almost

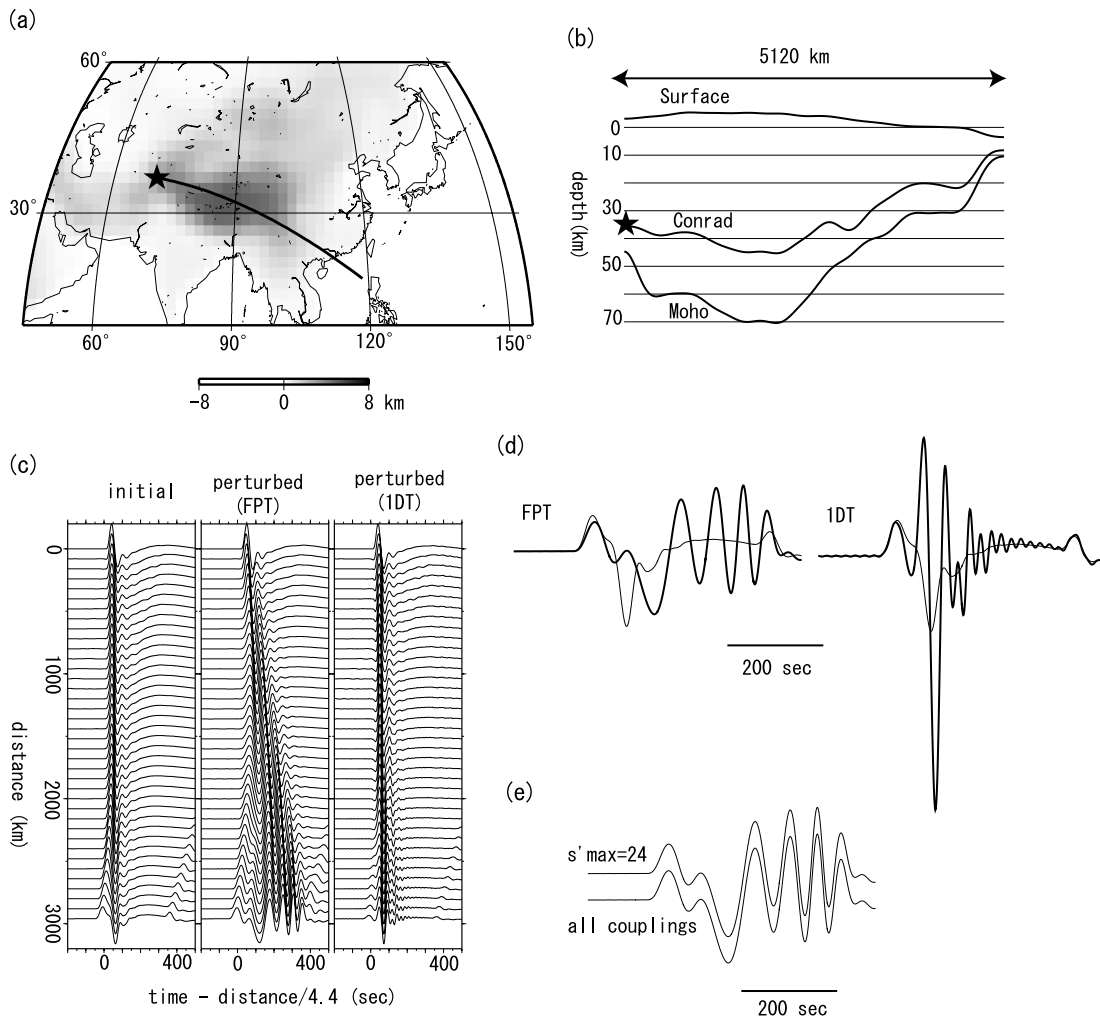


Figure 4. (a) The path on which the SH -wave propagations are simulated (thick solid line). The star shows the location of the source. Surface (or bathymetry) topography of Crust 2.0 model (Bassin *et al.* 2000) are overlapped by black-and-white colour scale. (b) The crustal topography model used as the perturbed model in this simulation to represent the Crust 2.0 model on the thick solid line in (a). The star shows the location of the source used with this perturbed model. (c) The record section computed for the initial model (left), for the perturbed model by using finite perturbation theory (FPT; middle) and for the perturbed model by using first-order perturbation theory (1DT; right). The vertical axis shows the distance from the epicentre and the horizontal axis shows the reduced time by $4.4^{-1} \text{ s km}^{-1}$. The amplitude is normalized by the maximum amplitude of each trace. (d) Synthetic seismograms for the initial model (thin solid line) and for the perturbed model (thick solid line) at 2960 km from the epicentre computed by using FPT (left) and 1DT (right). (e) The synthetic seismograms for the perturbed model computed by using FPT and the approximation of eq. (68) ($s'_{\max} = 24$; upper), and by using FPT and considering all couplings between every pair of the trial functions used (lower).

$\pi/4$ and anomalously large amplitude perturbation for the main surface wave packet. This feature is very close to that shown in Fig. 3(c) and indicates that 1DT breaks down for this realistic problem. Note that this does not mean that the formulations by Woodhouse (1980) are inappropriate, because the author probably considered only lower frequency problems such as the free oscillations of the Earth. The only conclusion here is that we need extensions to the previous formulations when we want to solve higher frequency problems than those assumed in the previous formulations.

Finally, we confirm that the effect of truncation in the expansion of eq. (68) is small. Fig. 4(e) shows the comparison between the synthetic seismogram at $x = 2960 \text{ km}$ computed by truncating the expansion in eq. (68) at $s'_{\max} = 24$ and the synthetic seismogram in Fig. 4(d) (computed by FPT considering all couplings between every pair of trial functions used). Because s_{\max} in eq. (65) is also 24, under this approximation, the number of non-zero matrix elements in $\delta\mathbf{H}$ of eq. (70) does not increase as a result of the non-linear term. However, as we see in Fig. 4(e), the obtained synthetic seismograms are almost identical. This fact indicates that the approximation of eq. (68) achieves both accuracy of synthetic seismograms and efficiency of computation, and should be useful in the applications to waveform inversion studies of Earth structure.

4.3 Extension to the spherical case

The above formulation is for the Fourier basis. Extension to the spherical harmonics (i.e. extension to the spherical coordinate) is straightforward. We express the equation of motion for the initial model (eq. 1 for the Cartesian coordinates case) in (r, θ, ϕ) and the equation of motion for

the perturbed model (eq. 2 for the Cartesian coordinates case) in (r', θ', ϕ') . We denote the mapping (eq. 19 for the Cartesian coordinates) from (r, θ, ϕ) to (r', θ', ϕ') as

$$\begin{cases} r' = r + \delta R(r, \theta, \phi) \\ \theta' = \theta \\ \phi' = \phi. \end{cases} \quad (82)$$

The perturbation of the matrix elements (eqs 22 and 32 for the Cartesian coordinate case) as a result of δR in eq. (82) is as follows:

$$\delta T_{mn} = \int_V [\phi_i^{(m)}]^* \rho \phi_i^{(n)} \delta R_{|r} dV, \quad (83)$$

$$\begin{aligned} \delta H_{mn} &= \int_V [\phi_{i|j}^{(m)}]^* C_{ijkl} \phi_{k|l}^{(n)} \delta R_{|r} dV \\ &\quad - \int_V \{ [\phi_{i|r}^{(m)}]^* C_{ijkl} \phi_{k|l}^{(n)} \delta R_{|j} + [\phi_{i|j}^{(m)}]^* C_{ijkl} \phi_{k|r}^{(n)} \delta R_{|l} \} dV \\ &\quad + \int_V [\phi_{i|r}^{(m)}]^* C_{ijkl} \phi_{k|r}^{(n)} \frac{\delta R_{|j} \delta R_{|l}}{1 + \delta R_{|r}} dV, \end{aligned} \quad (84)$$

where $|$ denotes the physical derivatives (e.g. $|j$ denotes the derivatives with respect to the local Cartesian coordinates in the j direction) and dV denotes the volume element in spherical coordinates, $r^2 \sin \theta dr d\theta d\phi$.

When we use the vector spherical harmonics as the horizontally dependent part of the trial functions $\phi_i^{(n)}$, we can evaluate the matrix elements of eqs (83) and (84) in the same fashion as that used in the 2-D *SH* problem in Section 4.1. We expand the perturbation, δR in eq. (82), in terms of the linear spline functions for the vertically dependent part and the spherical harmonics for the laterally dependent part, as follows:

$$\delta R(r, \theta, \phi) = \sum_k \sum_{s=0}^{s_{\max}} \sum_{t=-s}^s \delta r_{kst} X^{(k)}(r) Y^{(st)}(\theta, \phi), \quad (85)$$

where δr_{kst} are the expansion coefficients and $Y^{(st)}$ are the spherical harmonics.

In eqs (83) and (84), only the last term of right-hand side of eq. (84) is non-linear to δR and the other terms are linear. The laterally dependent part of the linear terms can be expressed by a product of three generalized spherical harmonics (Phinney & Burridge 1973), which can be evaluated using the Wigner 3-J symbol (e.g. Edmonds 1960) or the J-square symbol (e.g. Smith 1974). To evaluate the higher order term, we re-expand it in terms of the spherical harmonics and truncate it at the angular order, s'_{\max} :

$$\frac{\delta R_{|j} \delta R_{|l}}{1 + \delta R_{|r}} = \sum_{k'} \sum_{s'=0}^{s'_{\max}} \sum_{t'=-s'}^{s'} \delta r'_{k's't'} Q_{jl}^{(k')}(r) Y^{(s't')}(\theta, \phi), \quad (86)$$

where $\delta r'_{k's't'}$ are the expansion coefficients and $Q_{jl}^{(k')}(r)$ are some vertically dependent functions. Using this expansion, the non-linear term can be evaluated in the same fashion as the linear terms. Note that the equation of motion in terms of the spherical harmonics is related to the equation of motion in terms of the Fourier basis via the Earth flattening transformation, and the useful approximation for the Fourier basis should also be useful for the spherical harmonics.

5 DISCUSSION

In this paper, we derive the exact matrix operators \mathbf{T}' and \mathbf{H}' in eqs (21) and (31) (or in eqs 22 and 32) for the finite boundary perturbation problem in contrast to previous studies, which have derived the operators by using 1DT. In the numerical examples in this paper, we showed that 1DT breaks down for surface waves with a period of 50 s in a realistic problem. In recent waveform inversion studies (e.g. Megnin & Romanowicz 2000; Takeuchi & Kobayashi 2004), the body waves for this frequency range are used as a data set, but the surface waves for this frequency range are excluded. This is mainly a result of the insufficient accuracy of 1DT for computing the effect of crustal heterogeneities. Our method can compute accurate synthetic seismograms for arbitrary frequency ranges and should be better able to retrieve the information in the surface waves of higher frequencies.

In our formulations, we ignore the effect of self-gravity and Earth rotation. Extension to include these effects is a topic of future research. As was shown in Woodhouse & Dahlen (1978), the boundary conditions at the solid–liquid boundaries should be a prime topic.

In this paper, we do not discuss discretization. Geller & Takeuchi (1995) proposed the optimally accurate matrix operators for \mathbf{T} and \mathbf{H} in eq. (11) to optimize the performance of the computation. Deriving the optimally accurate operators for \mathbf{T}' and \mathbf{H}' in eq. (12) (i.e. the optimally accurate operators for eqs 21 and 31) is also an important research topic. They can be straightforwardly derived for the *SH* problem and we have already used them in the numerical examples shown herein. However, we should newly design the operators for the *P–SV* problem and the 3-D heterogeneous problem. With regard to the external force term, \mathbf{g} in eq. (11) and (12), Takeuchi & Geller (2003) proposed an accurate discretization. If we use these accurate discretization methods together with the finite boundary perturbation theory presented in this paper, we should be able to further improve the accuracy of crustal correction.

ACKNOWLEDGMENTS

This research was partly supported by grants from the Japanese Ministry of Education, Culture, Sports, Science and Technology (Nos 16740249 and 14540393). This is Berkeley Seismological Laboratory contribution #05-02.

REFERENCES

- Aki, K. & Larner, K.L., 1970. Surface motion of a layered medium having an irregular interface due to incident plane SH waves, *J. geophys. Res.*, **75**, 933–954 (AL).
- Bassin, C., Laske, G. & Masters, G., 2000. The current limits of resolution for surface wave tomography in North America, *EOS, Trans. Am. geophys. Un.*, **81**, Fall Meet. Suppl., Abstract S12A-03.
- Cummins, P.R., Geller, R.J., Hatori, T. & Takeuchi, N., 1994. DSM complete synthetic seismograms: SH, spherically symmetric, case, *Geophys. Res. Lett.*, **21**, 533–536.
- Cummins, P.R., Takeuchi, N. & Geller, R.J., 1997. Computation of complete synthetic seismograms for laterally heterogeneous models using the Direct Solution Method, *Geophys. J. Int.*, **130**, 1–16.
- Dahlen, F.A. & Tromp, J., 1998. *Theoretical Global Seismology*, Princeton University Press, Princeton.
- Dziewonski, A.M. & Anderson, D.L., 1981. Preliminary reference Earth model, *Phys. Earth planet. Int.*, **25**, 297–356.
- Edmonds, A.R., 1960. *Angular Momentum in Quantum Mechanics*, Princeton University Press, Princeton.
- Geller, R.J. & Ohminato, T., 1994. Computation of synthetic seismograms and their partial derivatives for heterogeneous media with arbitrary natural boundary conditions using the Direct Solution Method, *Geophys. J. Int.*, **116**, 421–446.
- Geller, R.J. & Takeuchi, N., 1995. A new method for computing highly accurate DSM synthetic seismograms, *Geophys. J. Int.*, **123**, 449–470.
- Geller, R.J. & Takeuchi, N., 1998. Optimally accurate time-domain second-order finite difference scheme for the elastic equation of motion: 1-D case, *Geophys. J. Int.*, **135**, 48–62.
- Hara, T., Tsuboi, S. & Geller, R.J., 1993. Inversion for laterally heterogeneous Earth structure using iterative linearized waveform inversion, *Geophys. J. Int.*, **115**, 667–698.
- Kohketsu, K., 1987. 2-D reflectivity method and synthetic seismograms for irregularly layered structures—I. SH-wave generation, *Geophys. J. R. astr. Soc.*, **89**, 821–838.
- Komatitsch, D. & Tromp, J., 2002a. Spectral-element simulations of global seismic wave propagation—I. Validation, *Geophys. J. Int.*, **149**, 390–412.
- Komatitsch, D. & Tromp, J., 2002b. Spectral-element simulations of global seismic wave propagation—II. Three-dimensional models, oceans, rotation and self-gravitation, *Geophys. J. Int.*, **150**, 303–318.
- Komatitsch, D. & Vilotte, J.P., 1998. The spectral element method: an efficient tool to simulate the seismic response of 2D and 3D geological structures, *Bull. seism. Soc. Am.*, **88**, 368–392.
- Li, X.D. & Tanimoto, T., 1993. Waveforms of long-period body waves in a slightly aspherical Earth model, *Geophys. J. Int.*, **112**, 92–102.
- Lognonné, P. & Romanowicz, B., 1990. Modeling of coupled normal modes of the Earth: the spectral method, *Geophys. J. Int.*, **102**, 365–395.
- Lysmer, J. & Drake, L.A., 1972. A finite element method for seismology, *Meth. Comput. Phys.*, **11**, 181–216.
- Megnin, C. & Romanowicz, B., 2000. The three-dimensional shear velocity structure of the mantle from the inversion of body, surface and higher-mode waveforms, *Geophys. J. Int.*, **143**, 709–728.
- Mizutani, H., 2001. Accurate and efficient methods for calculating synthetic seismograms when elastic discontinuities do not coincide with the numerical grid, *D. Sc. thesis*, University of Tokyo, Tokyo.
- Phinney, R.A. & Burridge, R., 1973. Representation of the elastic-gravitational excitation of a spherical earth model by generalized spherical harmonics, *Geophys. J. R. astr. Soc.*, **34**, 451–487.
- Priolo, E., Carcione, J.M. & Seriani, G., 1994. Numerical simulation of interface waves by high-order spectral modeling techniques, *J. acoust. Soc. Am.*, **95**, 681–693.
- Smith, M.L., 1974. The scalar equations of infinitesimal elastic-gravitational motion for a rotating, slightly elliptical Earth., *Geophys. J. R. astr. Soc.*, **37**, 491–526.
- Takeuchi, N. & Geller, R.J., 2000. Optimally accurate second-order time-domain finite difference scheme for computing synthetic seismograms in 2-D and 3-D media, *Phys. Earth planet. Int.*, **119**, 99–131.
- Takeuchi, N. & Geller, R.J., 2003. Accurate numerical methods for solving the elastic equation of motion for arbitrary source locations, *Geophys. J. Int.*, **154**, 852–866.
- Takeuchi, N. & Kobayashi, M., 2004. Improvement of Seismological Earth Models by Using Data Weighting in Waveform Inversion, *Geophys. J. Int.*, **158**, 681–694.
- Takeuchi, N., Geller, R.J. & Cummins, P.R., 1996. Highly accurate P-SV complete synthetic seismograms using modified DSM operators, *Geophys. Res. Lett.*, **23**, 1175–1178.
- Takeuchi, N., Geller, R.J. & Cummins, P.R., 2000. Complete synthetic seismograms for 3-D heterogeneous Earth models computed using modified DSM operators and their applicability to inversion for Earth structure, *Phys. Earth planet. Int.*, **119**, 25–36.
- Tsuboi, S., Komatitsch, D., Ji, C. & Tromp, J., 2003. Broadband modeling of the 2002 Denali fault earthquake on the Earth Simulator, *Phys. Earth planet. Int.*, **139**, 305–312.
- Woodhouse, J.H., 1976. On Rayleigh's principle, *Geophys. J. R. astr. Soc.*, **46**, 11–22.
- Woodhouse, J.H., 1980. The coupling and attenuation of nearly resonant multiplets in the Earth's free oscillation spectrum, *Geophys. J. R. astr. Soc.*, **61**, 261–283.
- Woodhouse, J.H. & Dahlen, F.A., 1978. The effect of a general aspherical perturbation on the free oscillations of the Earth, *Geophys. J. R. astr. Soc.*, **53**, 335–354.
- Woodhouse, J.H. & Dziewonski, A.M., 1984. Mapping the upper mantle: three-dimensional modeling of Earth structure by inversion of seismic waveforms, *J. geophys. Res.*, **89**, 5953–5986.